Proceedings of the ASME 2012 International Design Engineering Technical Conferences &
Computers and Information in Engineering Conference
IDETC/CIE 2012
August 12-15, 2012, Chicago, IL, USA

DETC2012-70290

OPTIMIZATION OF WIND FARM LAYOUT AND WIND TURBINE GEOMETRY USING A MULTI-LEVEL EXTENDED PATTERN SEARCH ALGORITHM THAT ACCOUNTS FOR VARIATION IN WIND SHEAR PROFILE SHAPE

Bryony L. DuPont
Integrated Design Innovation Group
Department of Mechanical Engineering
Carnegie Mellon University
Pittsburgh, PA 15232
Email: bryony@cmu.edu

Jonathan Cagan
Integrated Design Innovation Group
Department of Mechanical Engineering
Carnegie Mellon University
Pittsburgh, PA 15232
Email: cagan@cmu.edu

Patrick Moriarty
National Wind Technology Center
National Renewable Energy Laboratory
Boulder, CO 80303
Email: patrick.moriarty@nrel.gov

ABSTRACT

This paper presents a multi-level Extended Pattern Search algorithm (EPS) to optimize both the local positioning and geometry of wind turbines on a wind farm. Additionally, this work begins to draw attention to the effects of atmospheric stability on wind farm power development. The wind farm layout optimization problem involves optimizing the local position and size of wind turbines such that the aerodynamic effects of upstream turbines are reduced, thereby increasing the effective wind speed at each turbine, allowing it to develop more power. The extended pattern search, employed within a multi-agent system architecture, uses a deterministic approach with stochastic extensions to avoid local minima and converge on superior solutions compared to other algorithms. The EPS presented herein is used in an iterative, hierarchical scheme – an overarching pattern search determines individual turbine positioning, then a sub-level EPS determines the optimal hub height and rotor for each turbine, and the entire search is iterated. This work also explores the wind shear profile shape to better estimate the effects of changes in the atmosphere, specifically the changes in wind speed with respect to height on the total power development of the farm. This consideration shows how even slight changes in time of day, hub height, and farm location can impact the resulting power. The objective function used in this work is the maximization of profit. The farm installation cost is estimated using a data surface derived from the National Renewable Energy Laboratory (NREL) JEDI wind model. Two wind cases are considered: a test case utilizing constant wind speed and unidirectional wind, and a more realistic wind case that considers three discrete wind speeds and varying wind directions, each of which is represented by a fraction of occurrence. Resulting layouts indicate the effects of more accurate cost and power modeling, partial wake interaction, as well as the differences attributed to including and neglecting the effects of atmospheric stability on the wind shear profile shape.

INTRODUCTION

As the population of the world grows and sources of fossil fuels such as coal and natural gas dwindle and become more difficult and costly to access (as well as a major cause of greenhouse gas emissions), it is imperative that clean alternative energies, such as wind power, are thoroughly explored. Increasing the incorporation of wind power into the national power development scheme will help to fulfill the substantial increase in power the United States is projected to require – a 39% increase over the next 20 years. Additionally, the United States Department of Energy has presented the challenge to meet 20% of the U.S. total electricity demand via wind power by the year 2030 [1]. To meet this challenge and to purvey the merits of wind technology, it is important that newly developed wind farms are performing optimally, that is; they develop as much power as possible, given local wind conditions of the proposed site, turbine geometry, and site characteristics.

The EPS algorithm has been previously applied to optimize wind turbine micrositing [2] (the positions of wind turbines within a farm), and the current work expands the problem formulation to further prove the effectiveness of the EPS algorithm and to create farm layouts that more accurately account for actual wind conditions. A new cost model is proposed, based on an extensive NREL report [3] that estimates cost based on the parameters of turbine rotor radius and hub height. The two-parameter cost model is possible due to the incorporation of wind shear into the effective wind speed calculations. Wind shear is the variance of velocity based on height from the ground, and is represented mathematically by the power law. Unlike many previous wind farm optimizations that treat turbine rotors as points, we consider the effects of partial wake interaction across the rotor swept area. A systematic approach is taken to statistically determine the rotor-averaged wind speed created by partial wake interaction, and the sub-level rotor radius EPS algorithm can accordingly adjust the rotor swept area to aid in the optimization of cost and power development. Additionally, some of the effects of atmospheric stability are considered by accounting for the change in wind shear profile shape based on time of day and season.

In addition, the EPS is installed within a multi-agent system to account for each turbine's design activities. The agent approach is advantageous given that it facilitates multiple objectives and its architecture is highly adaptable, such that agents can be removed, added, or manipulated easily, without altering other facets of the code

[4]. This will be particularly beneficial considering proposed future EPS work, which will account for the dynamic nature of the wind farm layout problem as new technologies, turbine designs, and local environmental factors are considered.

PREVIOUS APPROACHES

The optimization of wind farm layouts can be based on many factors, though previous literature generally focuses on maximizing the power development of the farm while minimizing cost. The first computational optimization approach to the wind farm layout optimization problem was performed by Mosetti et al. in 1994 [5], who set up the framework upon which many future optimization schemes were based. Within a genetic algorithm (GA) approach, Mosetti et al. used chromosomal strings to create a discretized grid solution space. Grady et al. [6] improved upon this preliminary work primarily by exploiting greater computational resources, allowing their GA to give superior results. Both of these optimizations utilized the 2-D PARK model developed by Jensen [7] and minimize the objective of total cost of the farm while simultaneously maximizing power development.

As the most commonly utilized algorithm for the wind farm layout optimization problem, more advanced GA approaches have been widely applied, using a variety of objective functions and modeling approaches. A Distributed Genetic Algorithm (DGA) approach was developed by Huang [8]; while using the same discretized space and modeling as Mosetti et al. [5], the DGA was able to create layouts that develop more power, utilizing an objective function that maximized wind farm profit. Huang then improved on the DGA by creating a Hybrid-DGA approach [9] that used both global and local objective functions. Wang et al. [10] developed a GA that improved on the discretization of previous work by allowing for varying shapes and coarseness of the solution space. Similar approaches were developed by Sisbot et al. [11] and Emami et al. [12], which expanded the use of GAs to solve the wind farm layout optimization problem by separating total farm cost and power development into distinct objectives, creating multi-objective optimizations that allow for focus on initial farm costs. Kusiak et al. [13] developed a multi-objective evolutionary algorithm approach (similar to a GA) that maximized the annual energy production of the farm, a more accurate measure of farm cost than cost modeling used in previous work.

Approaches to solving the wind farm layout problem that utilize particle swarm optimization (PSO) are also relevant. PSO algorithms are related to both biological swarming behaviors and evolutionary computation, and were used by Wan et al. [14] and Chowdhury et al. [15] to solve the wind farm optimization problem. The latter researchers also considered varying turbine rotor geometries in their search [16]. Ozturk et al. [17] developed a different approach, a heuristic method, that utilized a weighted multi-objective function and a continuous solution space.

The current work builds on previous Extended Pattern Search research that has been applied to the wind farm layout optimization problem with success by DuPont and Cagan [2]. The previous application of EPS indicated that the combination of deterministic search and stochastic elements characteristic of the EPS were particularly well-suited to the multi-modal wind farm layout problem, allowing for the development of superior layouts than previous algorithms, including comparable genetic algorithms.

Improving upon previous work, we sought to more accurately model the cost of installation of operations and maintenance of a potential wind farm. Additionally, the effects of wind shear are not typically incorporated into the power development modeling used in wind farm layout optimization. The current paper addresses these deficiencies by using a cost model that is derived from the extensive NREL JEDI wind farm model [18], using more accurate power modeling that is dependent on turbine geometry and wind shear, and incorporating the effects of atmospheric stability. Additionally, new and varying turbine geometries are optimized, and a profit objective function is explored in order to better understand the tradeoffs between farm cost and farm power development.

MULTI-LEVEL EXTENDED PATTERN SEARCH

This work elaborates on the Extended Pattern Search (EPS) algorithm approach to wind farm layout optimization developed by DuPont and Cagan [2]. A pattern search is a purely deterministic search algorithm [19] that traverses potential solutions using a defined series of pattern directions. The search only allows each turbine agent to accept solutions for which there is a benefit to the objective evaluation. The extensions that give the extended pattern search its name are attributes that infuse stochasticity into the search, aiding in escaping local minima. Multiple stochastic extensions are used throughout the EPS. A randomized initial layout of turbines is used in order to establish a broad range of turbine locations while not explicitly assigning starting locations. Secondly, the search order is randomized such that no turbine's individual movement is favored over another. Thirdly, a popping algorithm is employed that will select the weakest turbines (based on power development) and attempt to assign them to a new random location, until a certain number of attempts are made or the turbine is relocated with a superior global evaluation. It has been shown that the EPS is well-suited to complex layouts problems [20], particularly the wind farm layout optimization problem where it performs better than comparable genetic algorithms [2].

We seek to enhance the performance capability of the EPS by making it multi-level – the primary EPS searches through turbine locations on a defined continuous solution space, while two secondary concurrent EPS algorithms search through varying hub heights and rotor diameters in order to select optimal individual turbine geometries. This allows the benefits of the EPS to be extended to both the wind farm micrositing problem and turbine geometry optimization. A flowchart depicting the basics of the multi-level EPS is included in Fig. 1.

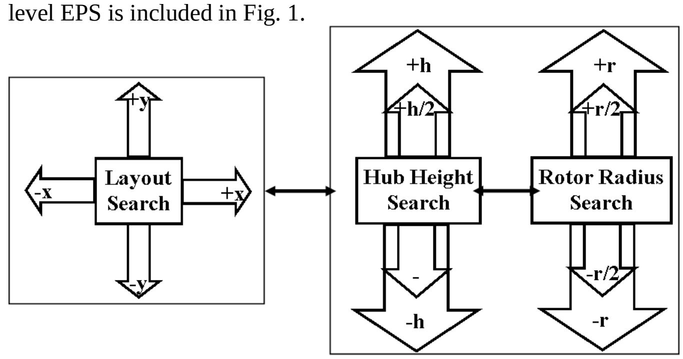

Fig. 1: FLOWCHART FOR MULTI-LEVEL EPS ALGORITHM

A set of four pattern search directions is followed for each of the individual EPSs. For the location EPS, the pattern directions are (+x, +y, -x, -y) in the x-y solution space. For each of the sub-level searches, the pattern directions are (+L, -L, +L/2, -L/2), where L represents a length in meters, either changing the height of the hub of the turbine in the z-direction or the radius of the rotor. At the start of each EPS, the pattern directions are traversed at a given step size, which is halved after no further movements are selected for that step size. The search exits after a minimum step size is reached, allowing the turbine agents to select both precise coordinates and geometries.

MULTI-AGENT SYSTEM METHODOLOGY

A multi-agent system is the collaboration of semi-autonomous software agents, loosely simulating the function of a human design team. Each agent represents a single purpose or specialty just as a single design engineer would have unique training or experience. Individually, agents work internally to meet their own particular goals. However, if given the means to communicate effectively within a group, a multi-agent system can interconnect and collectively work towards a balance between the global optimum and their individual objectives. The agents in the current system, which are both autonomous and capable of collaboration, are called collaborative agents [21]. Collaborative agents mimic the performance of a human design team, and it has been shown in previous work that, similar to a human design team, the solutions acquired by the collaborative agents may be superior than the sum of the capabilities of the individual agents involved [22]. The cooperation of agents representing strategies and capabilities grouped together in multi-agent systems has been shown to be very successful in solving engineering design problems in previous systems, such as A-Teams [23], A-Design [24], and blackboard systems [25].

In the current work, an individual agent represents a single turbine. The agent is equipped with memory capability for its current location, previous location, current and most recent previous geometric parameters, and current upstream and downstream turbines. An initial number of agents are created, with additional individual turbine agents added to determine layouts with the optimal number of turbines. The EPS is performed within one agent at a time, with each agent selecting its new potential locations, calculating the global objective, and determining whether to take a potential move. Additionally, each agent chooses a potential new hub height and rotor radius, evaluates globally, and determines whether or not to take on new geometry. Once an agent has completed an instance of the EPS, a new agent begins. The order in which the agents perform the EPS is randomized, which is one of the beneficial extensions of the EPS.

ATMOSPHERIC STABILITY

The atmospheric boundary layer, the portion of the atmosphere that is closest to the earth's surface and the region in which wind turbines are located, has physical attributes (temperature, wind direction, humidity, etc.) that can vary dramatically across the vertical range of a farm site. The stability of the atmospheric boundary layer is determined by the effects of temperature on airflow caused by the sun, cycling through the various stability conditions based on the time of day. Stable conditions occur when the temperature increases with height, often at night [26]. In the daytime, however, heat from the sun warms the ground and subsequently the air near the ground, creating an unstable atmospheric condition (the air is warmed from the ground up, causing warmer air to be situated below cooler air). This behavior creates significant atmospheric mixing that change the wind velocity and temperature gradients. Neutral stability conditions occur during the transition periods between stable and unstable.

The potential high turbulence in unstable conditions can cause rotor fatigue and early turbine failure [27]. Stable atmospheric conditions have the highest wind shear, and, depending on wind speed and turbine geometry, may prove to either increase or decrease the rotor-averaged effective wind speed [28].

Frandsen et al. [29] proposed that the effects of changes in atmospheric stability can greatly impact wind farm performance, including altering wind speed and turbulence. Work by Irwin [30], Hanafusa et al. [31], and Zoumakis et al. [32] explored how atmospheric stability and surface roughness affect the wind profile power-law exponent. Sumner and Masson [33] concluded that improper accounting for atmospheric stability using point estimations of the wind accounts for a 5% overestimation of the wind capacity of a site. Wharton and Lundquist [28] explored the errors that occur when only the power law is considered for determining the wind speed variation across a rotor swept area. These researchers used SODAR and cup anemometer measurements to define how the shape of the power law profile changes with atmospheric stability based on season.

As the secondary EPS allows for the optimization of both rotor radius and hub height, it is important to estimate the changes in wind speed based on distance from the ground. A rotor that is positioned at a higher hub height will generally see higher wind speeds, based on the influence of the boundary layer fluid flow, which is known as vertical wind shear and is represented by the power law:

$$U(z) = U(z_r)\left(\frac{z}{z_r}\right)^{\alpha_h}, \tag{1}$$

where $U_{(Z)}$ is the wind speed at hub height z, $U_{(Zr)}$ is the wind speed at a reference hub height z_r. The power law exponent α_h varies with time of day, season, mixing parameters and other factors.

In the current work, atmospheric stability is accounted for by averaging yearly wind shear exponent data from the Lamar Low-Level Jet Program (LLLJP) [34]. The wind shear exponent variation with height and month of the year is shown in Fig. 2.

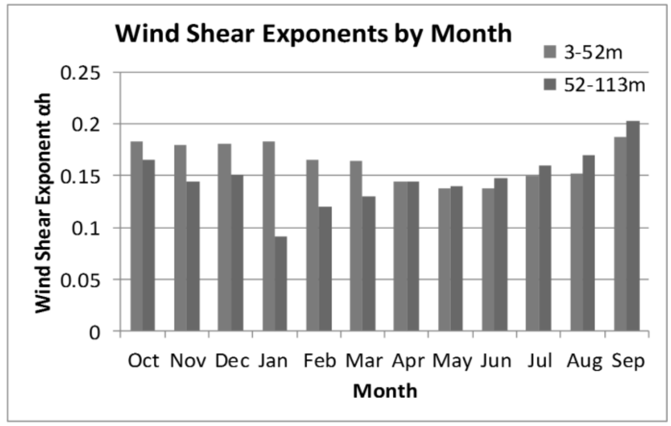

Fig. 2: WIND SHEAR EXPONENT BY MONTH [34]

In Fig. 2, the value α_h is the wind shear (or power law) exponent, where $\alpha_h = 0$ implies no shear across the rotor swept area and $\alpha_h = 0.3$ represents a very large shear. The average value for heights of 3 meters to 113m over the entire year is $\alpha_h = 0.15567$. There is no clear relationship determining whether low or high shear flow is optimal for turbine power development; rather it must also be dependent on wind speed, turbine geometry, and farm location.

In this work, we explore three optimal layouts for each of two wind cases: one layout using an average yearly power law exponent based on wind data from the LLLJP site given in Fig. 2 ($\alpha_h = 0.15567$), one layout using a low power law exponent ($\alpha_h = 0.1$) corresponding to unstable atmospheric stability conditions, and one layout using a higher power law exponent ($\alpha_h = 0.2$) corresponding to stable atmospheric stability conditions. Traditionally, a constant power law exponent value of $\alpha_h = 0.14$ is used, derived from flow over flat plates [35]. These results will explore how the change in the wind shear profile shape affects the resulting layout and turbine geometry optimization, and offer insight into the effects of using more site-accurate power law profile exponents instead of the traditional value of 0.14.

MODELING

A) Wake Modeling

In order to determine the amount of power a turbine is capable of developing, a 3-D extrapolation of the PARK wake model is used [7]. This wake model is a simplification of the complex aerodynamics involved with the motion of turbine blades rotating through air. This rotation causes a wake – an assumed conical-shaped area of air in which the flow is severely decremented immediately behind the rotor, but regains strength and asymptotically approaches the ambient wind speed downstream. This wake is modeled as triangular footprint in two dimensions, with both the width of the wake and the wind speed deficit being proportional to the distance downstream from the rotor, as illustrated in Fig. 3 and described by the momentum balance in Eq. (2):

$$\pi r_r^{\,2} v + \pi \left(r_1^{\,2} - r_r^{\,2} \right) U_0 = \pi r_1^2 U \,. \tag{2}$$

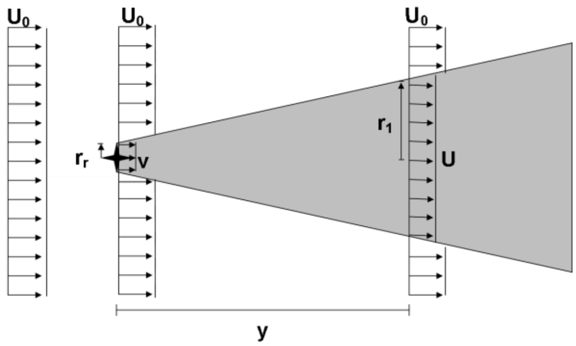

Fig. 3: DEPICTION OF (X,Y) TRIANGULAR WAKE

In Eq. 1, U_0 is the ambient wind speed, r_r is the radius of the turbine rotor, r_1 is the radial width of the wake at distance x downstream from the turbine, v is the severely decremented velocity directly behind the turbine (approximately 1/3 of the ambient wind speed), and U is the wind speed within the wake at distance downstream. U is a decremented representation of U_0 and is abstracted to be constant across the width of the wake (for the same value of y). The formula for U, the downstream wind speed within the wake, is given by:

$$U = U_0 \left(1 - \frac{2}{3} \left(\frac{r_r}{r_r + \alpha y} \right)^2 \right). \tag{3}$$

Equation 3 is used to determine the effective wind speed for any turbine that lies within one wake, where α is the entrainment constant, based on the turbine hub height z and the surface roughness z_0:

$$\alpha = \frac{0.5}{\ln\left(z / z_0 \right)} \quad . \tag{4}$$

A turbine that does not lie within a wake of an upstream turbine has an effective wind speed equal to the ambient wind speed approaching the farm. In the case of a turbine located in multiple wakes, it is necessary to sum the individual kinetic energy deficits of each of the n wakes to calculate the effective wind speed, as given by:

$$U = U_0 \left[1 - \sqrt{\sum_{i=1}^{n} \left(1 - \frac{U_i}{U_0} \right)^2} \right]. \tag{5}$$

In order to facilitate a more efficient search, a rectangular neighborhood in (x,y) is developed for each turbine to locate downstream turbines, using Eq. 4 to estimate the width of the wake. This equation relates the width of the wake to its downstream distance from the wake-producing turbine, based on the rotor radius:

$$r_1 = r_r + \alpha y \,. \tag{6}$$

Using the outermost points along the rotor swept area, a turbine will discern whether or not it is in the (x,y) rectangular neighborhood of an upstream turbine's wake, followed by a systematic approach to determine if the turbine lies within the frustum-shaped wake of the upstream turbine based on the 3-D extrapolation of the PARK model. The 3-D wake is depicted in Fig. 4.

Once turbine neighborhoods are established, an (x,z) view of each rotor is explored to determine the percentage of the rotor swept area that lies within each wake. Three distinct partial wake interaction scenarios are considered. The first is a turbine rotor that is partially located within the wake of one upstream turbine, or two upstream turbines whose wakes do not overlap across the rotor swept area. These scenarios are depicted in Fig. 5.

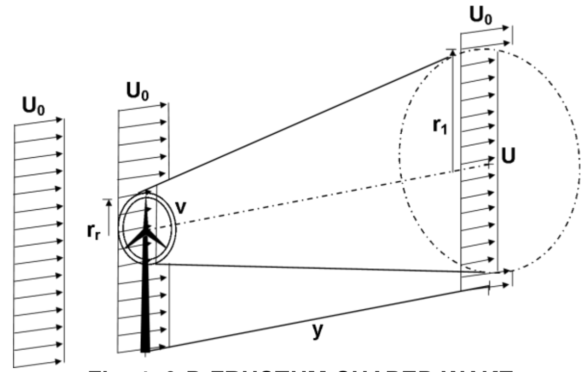

Fig. 4: 3-D FRUSTUM-SHAPED WAKE

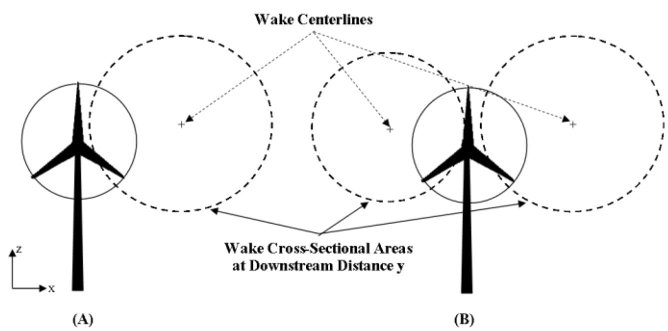

Fig. 5: TURBINE WITH PARTIAL WAKE INTERACTION, (A) WITH ONE PARTIAL WAKE, (B) WITH TWO DISTINCT PARTIAL WAKES

In either of the cases depicted in Fig. 5, the search algorithm determines if the turbine rotor has a partially interacting wake by calculating the distance between the hub of the turbine in question and the centerline of the wake:

$$d_{r-w} = \sqrt{\left(x_t - x_w \right)^2 + \left(z_t - z_w \right)^2} \quad , \tag{7}$$

where x_t and z_t are the x- and z-coordinates of the turbine hub, and x_w and z_w are the x- and z-coordinates of the centerline of wake at downstream distance y. Using Eq. (6), the radius of the wake r_w at the given downstream distance y can be calculated. Partial wake interaction can be verified using the following statements:

$$\begin{cases} d_{r-w} >= r_r + r_w & \text{Wake does not act on rotor swept area.} \\ d_{r-w} < r_r + r_w & \text{Wake acts on portion of rotor swept area.} \end{cases} \tag{8}$$

For the case of multiple distinct partial wakes, this check must be repeated to ensure that the wakes themselves do not overlap across the rotor swept area, and that they are in fact acting individually. Once partial wake interaction is verified, the formula for circle-circle intersection is used to calculate the area of the partial wake:

$$A_{Overlap} = r_r^{\,2} \cos^{-1}\left(\frac{d_{r-w}^{\;\;2} + r_r^{\,2} - r_w^{\,2}}{2 d_{r-w} r_r} \right) + r_w^{\,2} \cos^{-1}\left(\frac{d_{r-w}^{\;\;2} + r_w^{\,2} - r_r^{\,2}}{2 d_{r-w} r_w} \right) \,. \tag{9}$$
$$- \frac{1}{2} \sqrt{\left(-d_{r-w} + r_r + r_w \right)\left(d_{r-w} + r_r - r_w \right)\left(d_{r-w} - r_r + r_w \right)\left(d_{r-w} + r_r + r_w \right)}$$

With the area of the acting wake(s), one can determine the percentage of the rotor swept area that is affected by the wake(s):

$$\% = \frac{A_{Overlap}}{\pi r_r^{\,2}}. \tag{10}$$

With this percentage calculated, the effective wind speed is then determined for the areas that are affected by a wake or wakes using Eq. 3, and the effective wind speed is multiplied by the percentage(s) of overlap. The remaining portion of the rotor swept area is multiplied by the ambient wind speed, and these values are summed to determine the total estimated effective wind speed for the turbine.

The second wake scenario is that of a turbine that is in two or more wakes that overlap across the rotor swept area, as depicted in Fig. 6.

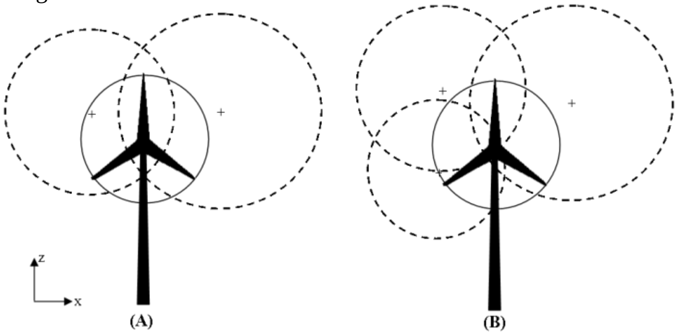

Fig. 6: TURBINE WITH OVERLAPPING PARTIAL WAKE INTERACTION, (A) WITH TWO WAKES, AND (B) WITH THREE WAKES

The percentage of wake overlap as depicted in Fig. 6 is not trivial to calculate, and as such determining the areas of overlap are avoided by applying a discretized mesh on the rotor swept area. The discretization shown is one of 49 points, which represent an evenly-spaced grid with a coarseness of ¼ of a rotor radius, as shown in Fig. 7:

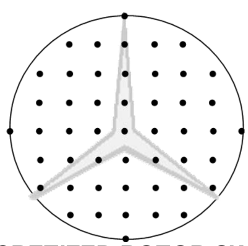

Fig. 7: DISCRETIZED ROTOR SWEPT AREA

At each of the discretized points, the effective wind speed can be calculated directly, by determining whether the point lies within an upstream wake or wakes. This is depicted in Fig. 8, where the point (x_i, z_i) is on the rotor swept area, and (x_w, z_w) are the coordinates of the centerline of a wake.

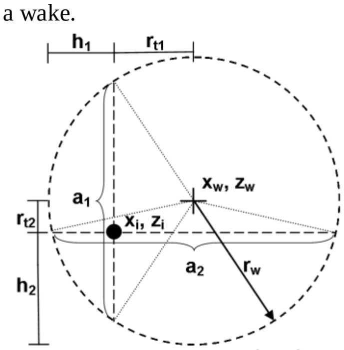

Fig. 8: POINT (x_i,z_i) WITHIN THE CIRCULAR CROSS-SECTIONAL AREA OF A WAKE

In Fig. 8, a_1 and a_2 are the chords of the circular wake cross-section that correspond to the x and z coordinates of the discrete point, h_1 and h_2 are the heights of the arced portion of the chord areas, and r_{t1} and r_{t2} are the heights of the triangular portion of the chord areas. r_{t1} and r_{t2} are simply the differences between the x- and z- coordinates of the discrete point and the centerline of the wake. It can be determined that:

$$h_1 = r_w - r_{t1} \quad \text{and} \quad h_2 = r_w - r_{t2}, \tag{11}$$

$$a_1 = 2\sqrt{h_1\left(2r_w - h_1\right)} \quad \text{and} \quad a_2 = 2\sqrt{h_2\left(2r_w - h_2\right)}. \tag{12}$$

With the heights and chord lengths calculated using Eq. (11) and Eq. (12), the following check will determine whether or not the discrete point lies within the wake:

$$z_w - \frac{a_1}{2} \le z_i \le z_w - \frac{a_1}{2} \quad \text{and} \quad \mathrm{x}_w - \frac{a_2}{2} \le x_i \le x_w - \frac{a_2}{2}. \tag{13}$$

If both of the statements in Eq. (13) are true, then the discrete point of the rotor swept area lies within the wake of the upstream turbine in question. This process is repeated for each of the 49 discrete points, and the effective wind speed is calculated based on the distance from, and the effective wind speed at, the upstream turbine(s) for each point (Eq.(2)). Each point then contributes $1/49^{\text{th}}$ of the total effective wind speed for the turbine.

An uncommon but nonetheless possible type of partial wake interaction is the case when the entire circular cross-sectional area of a wake lies within the rotor swept area, as depicted in Fig. 9.

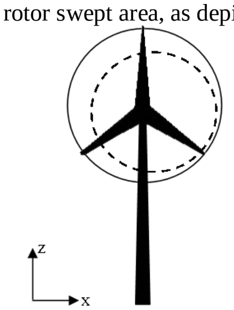

Fig. 9: TURBINE ROTOR SWEPT AREA WITH FULLY ENCLOSED WAKE

This type of partial wake interaction is unlikely due to wake propagation – as a wake travels downstream, its cross-sectional area becomes larger than its rotor swept area. This instance involves the cross-sectional area of the wake being smaller than the rotor swept area of a downstream turbine. To calculate the percentage of overlap for this case, the cross-sectional area of the wake is divided by the rotor swept area of the turbine, and the effective wind speed within the wake (calculated using Eq. (3)) is multiplied by that percentage. The remaining contribution to the turbine's effective wind speed is the remaining percentage multiplied by the ambient wind speed.

It should be noted that the use of this wake model suggests inherent simplification of the results, as the model itself uses an idealized semblance of the wake profile and behavior [36]. In particular, the wind speeds within a wake are considered constant across the width of the wake for a given downstream distance, whereas the lines of constant wind speed taking on the shape of a Gaussian distribution would be more accurate. Similarly, there is an "on/off" characteristic of the wake boundary that belies the more realistic wind speed gradient at the edges. Additionally, this model cannot account for the complex turbulent flow directly behind and caused by the rotor blades, and as such the wake effects of the near-wake region are unrealistic. However, given the minimum proximity constraint between turbines, this shortcoming most likely does not significantly affect the optimization. Regardless of these simplifications, the use of 3-D wake modeling improves upon previous wind farm optimization approaches that only utilize a 2-D representation of the wake and only consider turbines as point coordinates.

B) Power Modeling

Accurately reflecting the power production of a hypothetical wind farm is imperative in order to validate the results of a wind farm layout optimization. The current work uses power modeling that accounts for turbines of varying geometries, and as such employs power modeling given by Manwell et al. [35]:

$$P = \frac{1}{2}\rho A U^3 C_P \quad , \tag{14}$$

where ρ is the density of air (considered constant at 1.225 kg/m^3), A is the cross-sectional area swept by the rotor blades, U is the effective wind speed, and C_p is the power coefficient (which is relevant in the cubic region of the power curve shown in Fig. 10). The total power development of the farm is taken as the sum of the individual power outputs of each turbine. Additionally, we employed a power curve to more realistically represent the capability for turbines to develop power. When the wind speed is above the rated wind speed of 11.5 m/s, the turbine will only produce the amount of power it would at 11.5 m/s. The turbine will not produce power at wind speeds below the cut-in speed of 3 m/s, as shown in Fig. 10.

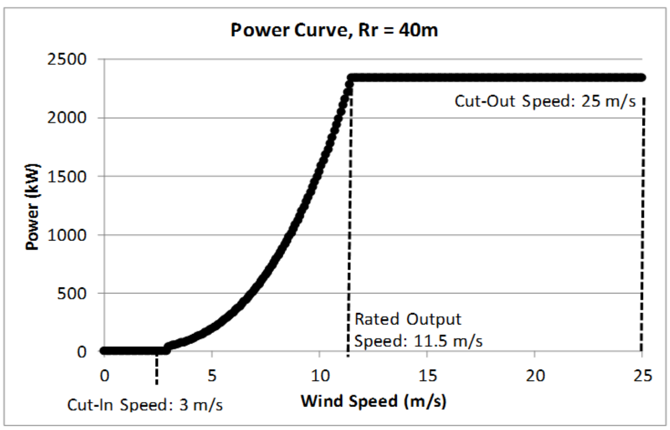

Fig. 10: POWER CURVE: POWER (kW) VERSUS WIND SPEED (m/s)

It should be noted that this algorithm deliberately allows for the selection of turbine geometries on a semi-continuous scale; that is, the search only allows for discrete values to be selected, but a very small terminating step size enables virtually any discrete value to be chosen. Turbine manufacturers, however, generally produce turbine families that use a set of available geometries, and are not as widely variable as those used in this study. The hub heights and rotor diameters in this work are constrained such that infeasible combinations of these parameters are impossible.

C) Cost Modeling

Accurately estimating the cost of installation of an onshore wind farm is a complex task that requires the consideration of a large number of variables. Clear contributors to cost include the materials and manufacturing for each individual turbine, land lease costs, infrastructure and electrical connectivity costs, but these are only a few of many. The National Renewable Energy Laboratory (NREL), sought to develop a means to estimate the costs associated with installation and operation and maintenance of both on and offshore wind farms, with projection capability for turbines of varying sizes and future installations [3]. NREL created a freely-available spreadsheet tool as part of the Jobs and Economic Development Impact (JEDI) model for wind power that predicts the cost of turbines based on a series of parameters that are user-configurable but default to researched values. Though the JEDI tool is not intended to predict the actual price of turbines (as that is a factor of the market and is highly variable), we use this work as a means to estimate the cost of the individual turbines on the farm such that the global objective function can minimize installation costs.

The JEDI model parameters vary based on U.S. state, and for our purposes have selected to locate our EPS-developed wind farms in Colorado (the LLLJP wind shear exponent data is also from data collection towers in Colorado). The year of construction is 2010, and the total project size is limited to the size of individual turbines. For the coupled input data of rotor radii (between 19 m and 56 m) and the effective wind speed compensated for hub height using the power law of Eq. (3) (between 38 m and 138 m), the power is developed using Eq. (14). These resulting calculated power evaluations are then used as input into the JEDI model for an individual turbine. The project cost results (the cost of installation) are used to create a cost 2nd-order polynomial surface that is dependent on rotor radius and hub height, as shown in Fig. 11.

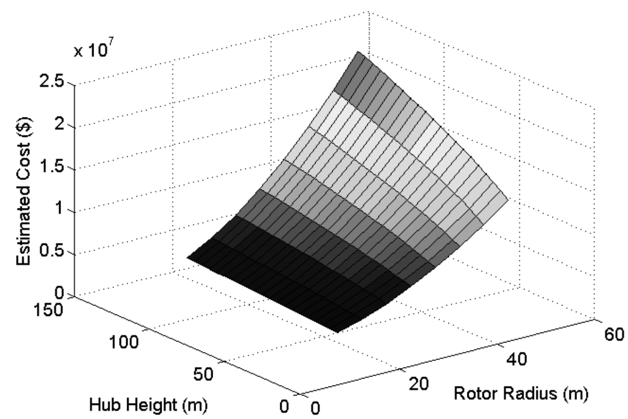

Fig. 11: POLYNOMIAL COST SURFACE AS A FUNCTION OF ROTOR RADIUS AND HUB HEIGHT: α_h = 0.15567

The cost surface depicted in Fig. 11 is estimated by the Eq. (15):

$$\begin{aligned} C(r,h) &= (2.454e+06) - (2.161e+05)\,r \\ &\quad -(1.203e+04)\,h + 6039r^2 + 2455rh - 161.2h^2. \end{aligned} \tag{15}$$

It should be noted that the polynomial cost surface is dependent on an input power, and is therefore dependent on the value of the power law exponent α_h. The formula stated in Eq. (15) pertains to the α_h value of 0.15567. These cost surfaces were developed by plotting 168 resulting cost points via a second-order polynomial surface fit. Compared to the cost modeling used in previous work [5,6] which was based solely on the number of turbines in each potential farm installation, the use of the NREL JEDI-derived cost surface is much more realistic and accurate.

The total project cost of the farm is taken as the sum of the project costs of each individual turbine as calculated by Eq. (15). The total power development of the farm is the sum of the individual turbine power outputs, as calculated in Eq. (14). With these two values, a global objective function was developed in order to accurately portray the interests of farm developers and researchers. This objective is the maximization of profit in dollars, formulated as the minimization of negative profit:

$$Objective = Cost_{\text{Project}} + Cost_{O\&M} \times t - Energy_{Yearly} \times t \times C_F \times COE \,, \tag{16}$$

where $Cost_{O\&M}$ is the annual operations and maintenance cost of the farm in \$/year, t is the amount of time (years) over which the cost is relevant, C_F is the capacity factor at which the farm performs, and COE is the cost of energy – the price at which a farm owner may sell the energy their farm develops, in \$/kWh. The operations and maintenance costs are estimated to be [3]:

$$Cost_{O\&M} = 0.007 \times Energy_{Yearly} \times t \times C_F \times COE \,. \tag{17}$$

The costs included are the initial project cost, which is generated by the cost surface given in Eq. (15), and the operations and maintenance costs per year, which are a function of the annual energy production of the farm. The annual energy production is the amount of power the farm can produce per year. The annual energy production multiplied by the price at which the power can be sold in \$/kWh gives the amount of money the farm can make.

NUMERICAL PROCEDURE

Two test cases are explored in this work. First, Case (a) is that of constant wind speed and unidirectional wind (from the bottom of the field in the $+y$ direction). Case (b) is a more accurate representation of wind site conditions, with three wind speeds (6, 9, and 12 m/s) and thirty-six wind directions (360° in 10° increments), with a probability of occurrence for each, depicted as a bar graph in Fig. 12.

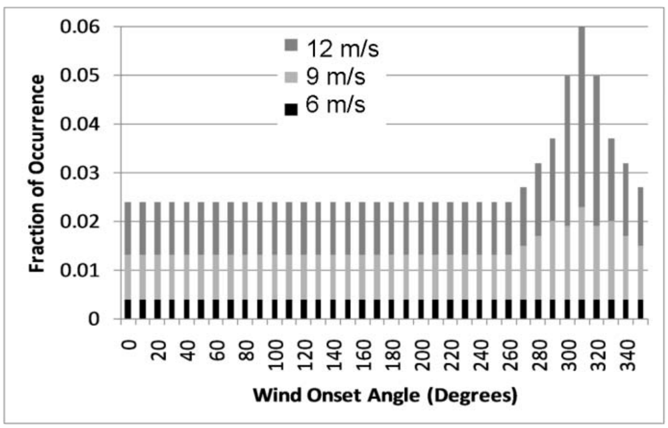

Fig. 12: FRACTION OF OCCURRENCE FOR WIND SPEEDS AND WIND DIRECTIONS – CASE (b)

The farm site is 2000 m x 2000 m with no topographical variance. The turbine geometry is initialized to an 80 m hub height with an 80 m rotor diameter. The multi-agent system performs over a continuous solution space, and as such every potential agent move first performs an interference check to ensure that it is not within 200 m radially of any other agent. Additionally, no agent is permitted to move itself out of the bounds of the farm area. After a random initial placement, each agent identifies any turbines that may lie upstream using a neighborhood search, and the distance to any potential upstream turbines. A check is performed to validate whether an agent lies in the wake of its potential upstream turbines, and the severity of the wake overlap. The agent then stores this information in order to calculate its own effective wind speed and power development. The initial step size of the coordinate EPS is chosen is 400 m and is halved until reaching a minimum value of 6.25 m. The sub-level Hub Height EPS algorithm uses an initial step size of 45 m, and is halved until reaching a minimum value of 1.4 m. The sub-level Rotor Radius EPS algorithm uses an initial step size of 25 m, and is halved until reaching a minimum value of 1.5 m. Feasible hub height values are between 38 m and 135 m, and feasible rotor radii are between 19 m and 67 m. The popping algorithm will attempt to relocate the 10 worst-performing turbines up to 100 random locations. A constant capacity factor of 0.4 is used [37], and cost of energy is taken to be 0.1 \$/kWh [8].

RESULTS

For both the simplified wind case (Case (a)) and the more realistic multidirectional wind case with varying wind speeds (Case (b)), the averaged value of $\alpha_h = 0.15567$ is compared to a lower value ($\alpha_h = 0.1$) and a higher value ($\alpha_h = 0.2$). These low and high values are similar to the minimum and maximum wind shear exponents gathered from wind data in Fig. 2, and will reveal more detail about how the changes in the wind shear exponent can affect the optimal layout and turbine geometry of a proposed wind farm site.

A preliminary parametric optimization was conducted in order to determine the optimal number of years over which the objective should be considered. For the averaged α_h value and 20 turbines, layouts were created using the profit objective for various numbers of years. The results of this study are summarized in Table 1.

Table 1: YEAR PARAMETRIC STUDY, α_h = 0.15567, 20 TURBINES

Years	Objective	Power (W)	Avg. Hub Height (m)	Avg. Rotor Radius (m)
10	1.27E+07	6.13E+06	38.516	19.129
15	2.14E+06	6.66E+06	39.641	19.723
16	-30151.1	7.18E+06	42.102	20.338
17	-2.93E+06	8.30E+06	46.25	21.407
20	-4.20E+07	6.64E+07	116.246	50.985

As this objective minimizes the negative profit, the farm costs are recouped and a profit is made (only applicable with the parameters presented) if the optimization is considered for at least 16 years. This estimation neglects many real-world factors that would significantly drive down the number of years until a farm is profitable, such as governmental incentives for renewable energy production and price negotiation from turbine manufacturers, which are not modeled in this work. It is interesting to note the differences in selected turbine geometry if the years over which the optimization is considered are increased – the longer the farm is expected to be producing power, the larger the turbine geometry the optimization selects. The optimization must be given enough time to recoup the higher project cost of larger turbines in order to consider using them. As a result of this parametric optimization, subsequent use of the profit objective will be considered over 20 years.

Case (a)

Evaluating the objective for the unidirectional, constant wind speed case, the ambient wind speed is taken to be 10 m/s, and the wind approaches the site in the $+y$ direction (from the bottom of the figure, upward). Using this simplified wind case helps explore the capability of the algorithm, and gives a clearer discernment of how the attributes of the search affect the result. For each value of α_h, resulting layout data were generated for layouts of 5-50 turbines. The objective function evaluation data were then plotted versus the number of turbines, and a cubic polynomial fit was applied; the minimum value for each curve is taken to be the optimal number of turbines for each α_h value (similar to the procedure performed in previous EPS work [2]). This gave an optimal value of 38 turbines for the $\alpha_h = 0.1$ case, 36 turbines for the $\alpha_h = 0.15567$ case, and 31 turbines for the $\alpha_h = 0.2$ case. These three layouts are shown in Fig. 14, Fig. 15, and Fig. 16, respectively, with a key to aid in interpretation of turbine geometry given in Fig. 13 (these symbols indicate ranges but each turbine's geometry is exact). Table 2 shows a comparison between the Case (a) results for $\alpha_h = 0.1$, $\alpha_h = 0.15567$, and $\alpha_h = 0.2$.

Table 2 : CASE (a) RESULTS

	αh = 0.1	αh = 0.15567	αh = 0.2
N	38	36	31
Objective Evaluation	-3.26156E+07	-4.43837E+07	-5.83643E+07
Total Power (MW)	57.6629	62.7362	79.3729
Avg. Turbine Hub Height (m)	70.21	79.98	95.29
Avg. Turbine Rotor Radius (m)	33.20	35.69	41.88

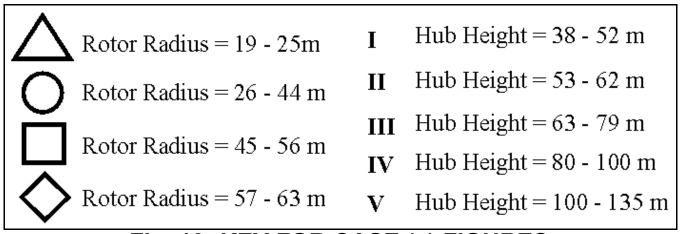

Fig. 13: KEY FOR CASE (a) FIGURES

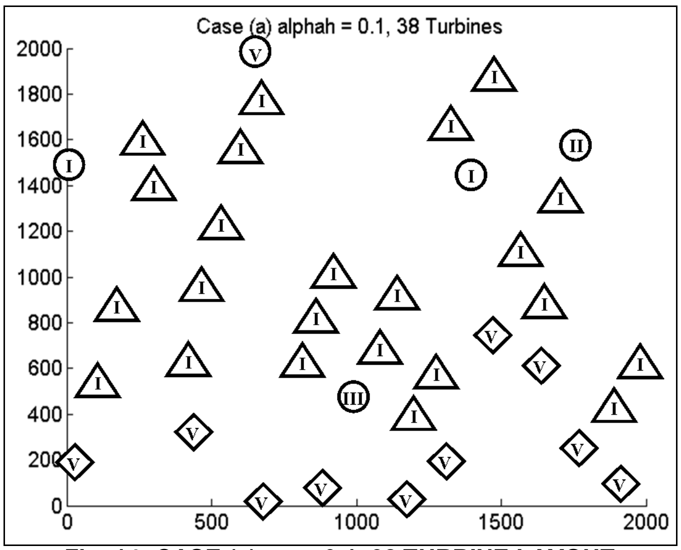

Fig. 14: CASE (a), α_h = 0.1, 38 TURBINE LAYOUT

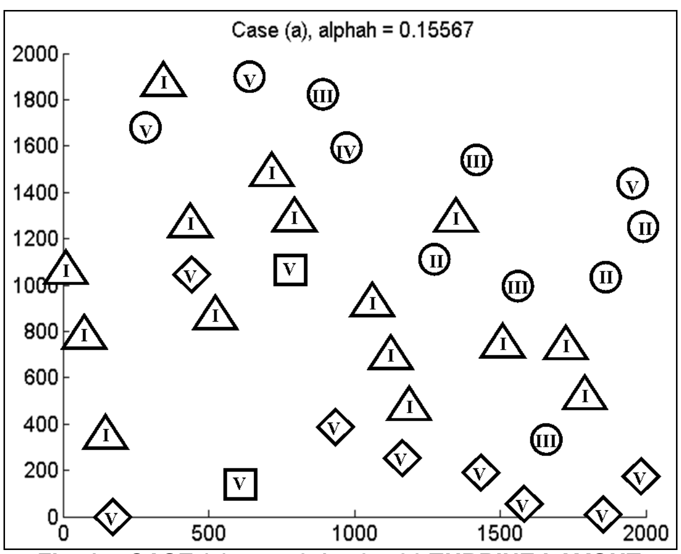

Fig. 15: CASE (a), α_h = 0.15567, 36 TURBINE LAYOUT

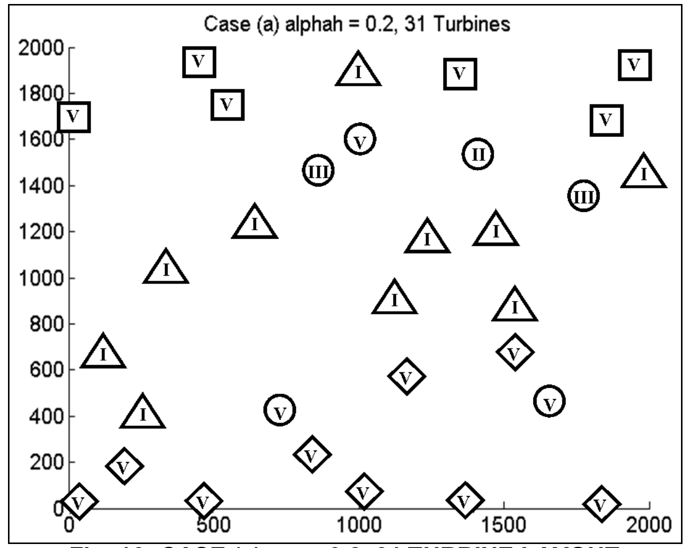

Fig. 16: CASE (a), α_h = 0.2, 31 TURBINE LAYOUT

These results show some interesting differences between the varying values of α_h. The lower α_h value influences an optimal layout with a greater number of turbines, but these turbines are generally smaller. The highest α_h value of 0.2 gives a layout with fewer turbines, but of significantly taller average turbine geometry. These results are consistent with our understanding of how the wind shear exponent influences the breadth of wind speeds. The ambient wind speed (10 m/s) is lower than, but close to the reference wind speed (11.5 m/s) for the power law calculation given in Eq. (1). This was deliberate to explore the incentive for turbines to increase their height or the size of their rotor swept areas, as doing so can result in an increase in power development, but will increase cost, potentially leading to an inferior objective evaluation. For all of the α_h values shown here, the largest possible turbine geometries were situated in the front of the field, with unobstructed ambient wind, where downstream turbines would select generally smaller geometries or taller hub heights to steer clear of an upstream wake or wakes. It must also be considered that turbine agents have selected relatively small turbine geometries due to the trade-off between cost and size. This also indicates the influence of including partial wake interaction – the smaller the rotor swept area, the less likely a turbine will produce a wake large enough to encompass others, and the less likely it will be located within a wake itself.

.

Case (b)

As with Case (a), the Case (b) results are summarized in Table 3, with α_h = 0.1, α_h = 0.15567, and α_h = 0.2 now used within the multidirectional variable wind speed case. These three layouts are shown in Fig. 17, Fig. 18, Fig. 19, respectively, with a turbine geometry symbol key given in Fig. 20.

Table 3: CASE (b) RESULTS

	αh = 0.1	αh = 0.15567	αh = 0.2
N	8	9	8
Objective Evaluation	-5.74532E+06	-6.90359E+06	-7.24115E+06
Total Power (MW)	9.92175	12.4051	12.5599
Avg. Turbine Hub Height (m)	75.87	78.36	80.00
Avg. Turbine Rotor Radius (m)	35.03	37.26	40.00

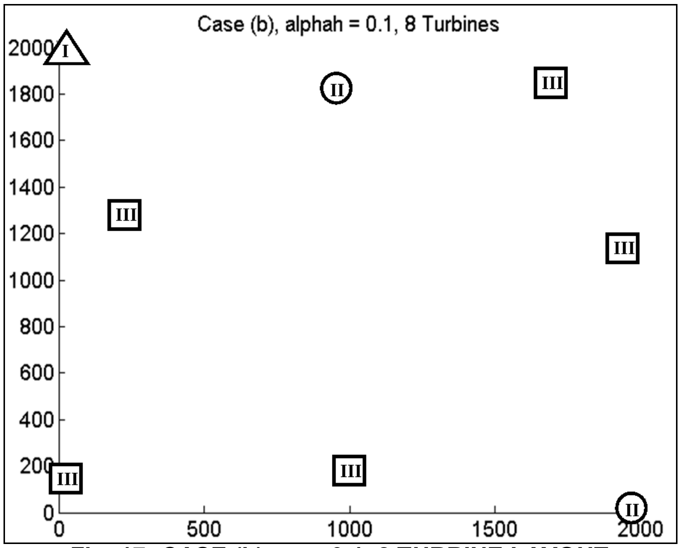

Fig. 17: CASE (b), α_h = 0.1, 8 TURBINE LAYOUT

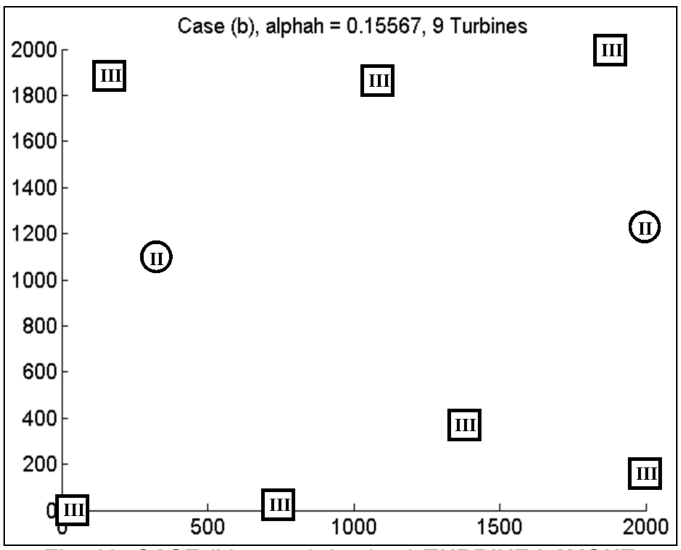

Fig. 18: CASE (b), α_h = 0.15567, 9 TURBINE LAYOUT

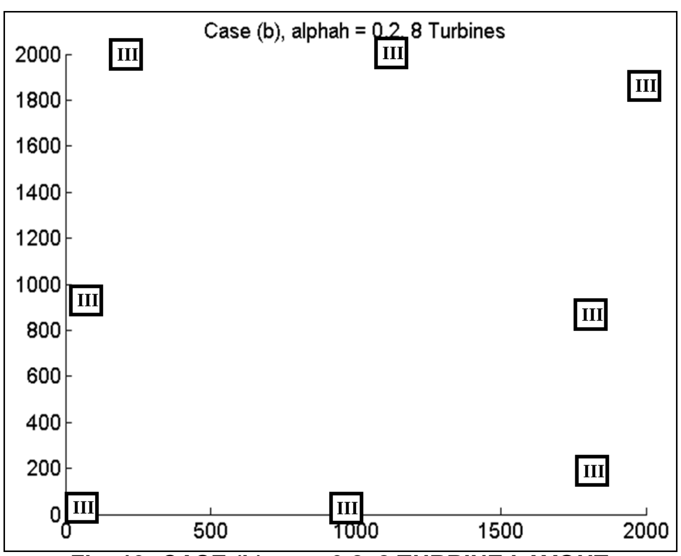

Fig. 19: CASE (b), α_h = 0.2, 8 TURBINE LAYOUT

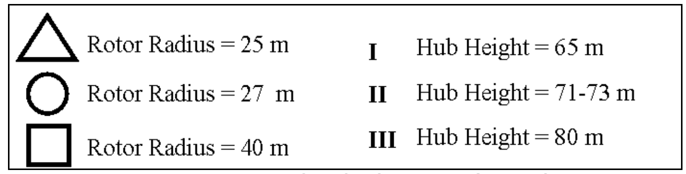

Fig. 20: KEY FOR CASE (b) FIGURES

The results for the multi-directional, varying wind speed case show consistency with previous work [2] in that the turbine agents, as the full rotation of wind directions doesn't enable movement outside of wakes, tend to be fewer in number, maximize their downstream distance, and migrate toward the outer field perimeter. Therefore, the decremented wind speed behind a rotor is given the distance needed to recover and approach its ambient speed. Unlike Case (a), there is no marked difference between the number of turbines stated in each optimal layout, though a clear pattern of optimal turbine geometries emerges. As with Case (a), the higher α_h = 0.2 value suggests larger turbine geometries, and the smaller α_h = 0.1 value influences a layout of smaller turbine geometries. This is due to the effect of the wind shear exponent on the wind shear profile shape – the larger exponent creates a more severe profile curve, with lower wind speeds at the ground and higher wind speeds at the top of the profile. The larger turbine geometries better capture this higher wind speed, and the higher resulting power development counteracts the higher cost of the larger geometry in the profit objective.

CONCLUDING DISCUSSION

The use of this advanced multi-level EPS algorithm builds on the previous wind farm layout optimization by incorporating more realistic variables and modeling in order to yield real-world applicable results. Enabling the optimization to select varying turbine geometries allows for a broader selection of possible layout designs and facilitates energy capture. In addition, this work shows the previously unexplored implications of realistic power and cost modeling on turbine size selection. The use of more accurate cost modeling has indicated the strong dependence of the objective on cost, where slight increases in turbine size can create scenarios where cost is no longer offset by the amount of power that is produced. Power modeling that accounts for changes in turbine geometry by incorporating the wind speed dependence on elevation are key to exploring farms not only of varying turbine geometries, but also of topographical variation. Additionally, it has been shown here that even slight variations in the power law exponent α_h can influence significant changes in proposed layouts and turbine geometry. This stresses the importance of undertaking exhaustive preliminary wind site testing in order to accurately capture wind shear behavior. We have also shown the impact of accounting for the productive life of the farm when using profit as an objective, as larger, more costly turbines are ideal if their initial investment cost is offset by significant productive time. The multi-level EPS algorithm built on a multi-agent system framework has proven to be highly effective for solving the wind farm layout optimization problem, delivering meaningful layouts that allow for adaptive turbine geometry.

ACKNOWLEDGEMENTS

This work was partially funded by the National Science Foundation under grants CMMI-0940730 and CMMI-0855326.

REFERENCES

[1] United States Department of Energy, 2008, 20% Wind by 2030, http://www.nrel.gov/docs/fy08osti/41869.pdf.

[2] DuPont B. L., and Cagan J., 2012, "An Extended Pattern Search Approach to Wind Farm Layout Optimization," ASME Journal of Mechanical Design, In Press.

[3] Fingersh L., Hand M., and Laxson A., 2006, Wind Turbine Design Cost and Scaling Model, National Renewable Energy Laboratory, Golden, CO.

[4] Orsborn S., and Cagan J., 2009, “Multiagent Shape Grammar Implementation: Automatically Generating Form Concepts According to a Preference Function,” Journal of Mechanical Design, **131**(12), pp. 121007-1 - 121007-10.

[5] Mosetti G., Poloni C., and Diviacco B., 1994, “Optimization of wind turbine positioning in large windfarms by means of a genetic algorithm,” Journal of Wind Engineering and Industrial Aerodynamics, **51**(1), pp. 105-116.

[6] Grady S. A., Hussaini M. Y., and Abdullah M. M., 2005, “Placement of wind turbines using genetic algorithms,” Renewable Energy, **30**(2), pp. 259-270.

[7] Jensen N. O., 1983, A Note on Wind Generator Interaction, Riso National Laboratory, Roskilde, Denmark.

[8] Huang H. S., 2007, “Distributed Genetic Algorithm for Optimization of Wind Farm Annual Profits,” 2007 International Conference on Intelligent Systems Applications to Power Systems, pp. 1-6.

[9] Huang H. S., 2009, “Efficient hybrid distributed genetic algorithms for wind turbine positioning in large wind farms,” 2009 IEEE International Symposium on Industrial Electronics, (ISlE), pp. 2196-2201.

[10] Wang F., Liu D., and Zeng L., 2009, “Study on computational grids in placement of wind turbines using genetic algorithm,” 2009 World Non-Grid-Connected Wind Power and Energy Conference, **2**, pp. 1-4.

[11] Sisbot S., Turgut O., Tunc M., and Camdali U., 2009, “Optimal Positioning of Wind Turbines on Gokceada Using Multi-Objective Genetic Algorithm,” Wind Energy.

[12] Emami A., and Noghreh P., 2010, “New approach on optimization in placement of wind turbines within wind farm by genetic algorithms,” Renewable Energy, **35**(7), pp. 1559-1564.

[13] Kusiak A., and Song Z., 2010, “Design of wind farm layout for maximum wind energy capture,” Renewable Energy, **35**(3), pp. 685-694.

[14] Wan C., Wang J., Yang G., and Zhang X., 2010, “Optimal Micro-siting of Wind Farms by Particle Swarm Optimization,” ICSI 2010, pp. 198-205.

[15] Chowdhury S., Zhang J., Messac A., and Castillo L., 2012, “Unrestricted wind farm layout optimization (UWFLO): Investigating key factors influencing the maximum power generation,” Renewable Energy, **38**(1), pp. 16-30.

[16] Chowdhury S., Messac A., Zhang J., Castillo L., and Lebron J., 2010, “Optimizing the Unrestricted Placement of Turbines of Differing Rotor Diameters in a Wind Farm for Maximum Power Generation,” ASME IDETC, Montreal, QC, Canada, pp. 1-16.

[17] Aytun Ozturk U., and Norman B. A., 2004, “Heuristic methods for wind energy conversion system positioning,” Electric Power Systems Research, **70**(3), pp. 179-185.

[18] NREL, “NREL JEDI Models,” http://www.nrel.gov/analysis/jedi/download.html.

[19] Torczon V., William C., and Trosset M. W., 1998, “From Evolutionary Operation to Parallel Direct Search : Pattern Search Algorithms for Numerical Optimization,” Computing Science and Statistics, pp. 396-401.

[20] Yin S., and Cagan J., 2000, “An Extended Pattern Search Algorithm for Three-Dimensional Component Layout,” ASME Journal of Mechanical Design, **122**, pp. 102-108.

[21] Nwana H. S., 1996, “Software Agents : An Overview,” Knowledge Engineering Review, **11**(3), pp. 205-244.

[22] Olson J., and Cagan J., 2004, “Interagent ties in team-based computational configuration design,” Artificial Intelligence for Engineering Design, Analysis, and Manufacturing, **18**, pp. 135-152.

[23] Talukdar S., Baerentzen L., Gove A., and Souza P. D., 1996, “Asynchronous Teams: Cooperation Schemes for Autonomous Agents,” Journal of Heuristics, **4**, pp. 295-321.

[24] Campbell M. I., Cagan J., and Kotovsky K., 1999, “A-Design- An Agent-Based Approach to Conceptual Design in a Dynamic Environment,” Research in Engineering Design, **11**, pp. 172-192.

[25] Nii H. P., 1986, “Blackboard Application Systems and a Knowledge Engineering Perspective,” AI Magazine, pp. 82-107.

[26] Rohatgi J., and Barbezier G. I. L., 1999, “Wind Turbulence and Atmospheric Stability - Their Effect on Wind Turbine Output,” Renewable Energy, **16**, pp. 908-911.

[27] Hiester T. R., and Pennell W. T., 1981, The Meteorological Aspects of Siting Large Wind Turbines, US Dept. of Energy.

[28] Wharton S., and Lundquist J. K., 2010, “Atmospheric Stability Impacts on Power Curves of Tall Wind Turbines - An Analysis of a West Coast North American Wind Farm,” Environmental Research Letters.

[29] Frandsen S., Antoniou I., Hansen J. C., Kristensen L., Chaviaropoulos B., Douvikas D., Dahlberg J. A., Derrick A., Dunbabin P., Hunter R., Ruffle R., Kanellopoulos D., and Kapsalis G., 2000, “Redefinition Power Curve for More Accurate Performance Assessment of Wind Farms,” Wind Energy, **3**, pp. 81-111.

[30] Irwin, 1979, “A Theoretical Variation of the Wind Profile Power Law Exponent as a function of Surface Roughness and Stability,” Atmospheric Environment, **13**, pp. 191-194.

[31] Hanafusa T., Lee C. B., and Lo A., 1986, “Dependence of the Exponent in Power Law Wind Profiles on Stability and Height Interval,” Atmospheric Environment, **20**(10), pp. 2059-2066.

[32] Zoumakis N. M., 1993, “The dependence of the power law exponent on surface roughness and stability in a neutrally and stably stratified surface boundary layer.pdf,” Atmosfera, **6**, pp. 79-83.

[33] Sumner J., and Masson C., 2006, “Influence of Atmospheric Stability on Wind Turbine Power Performance Curves,” Journal of Solar Energy Engineering, **128**(4), p. 531.

[34] Kelley N., Shirazi M., Jager D., Wilde S., Adams J., Buhl M., Sullivan P., and Patton E., 2004, Lamar Low-Level Jet Project Interim Report, Golden, CO.

[35] Manwell J. F., McGowan J. G., and Rogers A. L., 2009, Wind Energy Explained: Theory, Design and Application, John Wiley and Sons, West Sussex, United Kingdom.

[36] Katic I., Hojstrup J., and Jensen N. O., 1986, “A Simple Model for Cluster Efficiency,” European Wind Energy Association Conference and Exhibition, Rome, Italy, pp. 407-410.

[37] Renewable Energy Research Laboratory, 2009, “Wind Power: Capacity Factor, Intermittency, and What Happens When the Wind Doesn’t Blow?,” University of Massachusetts at Amherst, pp. 1-4.

